# Determining Electrostatic Properties of a Material Defined Double Quantum Dot

Anton Johansson (97antjoh@gmail.com)
Supervisor: David Barker (david.barker@ftf.lth.se)

December 18, 2019

## 1 Introduction

Double Quantum Dots (DQDs) are often introduced as a natural extension of single dot systems, and for good reason. Weil, et al. makes the analogy to atoms versus molecules for single versus double and even multiple dot systems [1]. In comparison to regular molecules however, DQDs allow for fine-grained control of electronic states and transitions, and compelling modern quantum mechanical problems are brought to light, including qubits and quantum computing among other things [1, 2].

When it comes to practise, however, problems naturally arise. A common approach to creating DQDs is by electrostatically defining potential barriers in an already low-dimensional system via external gates, simplicity notwithstanding, the resulting dots are not well defined due to the smooth barriers and moreover external noise is introduced via the gates which interferes with the quantized states [3].

This study focuses on material defined DQDs using a semiconductor heterostructure, giving well defined potential barriers in the conduction band, as described in Ref. [3]. Thus sidestepping the problems above. Figure 1 shows a schematic representation of one such DQD where $V_{SD}$ is the applied bias, $V_g^{(1,2)}$ and $C_g^{(1,2)}$ are the capacitive gate connections for dot 1 and 2 respectively. The tunnel barriers are modeled as a capacitor and resistor in parallel. Note that the superscript $(i)$ refers to variables with respect to the i:th dot.

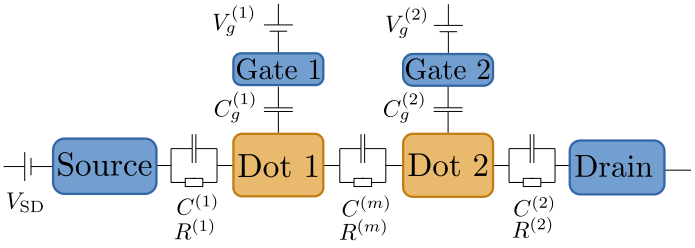


Figure 1: Schematic of double quantum dot with tunnel barriers and individual gates per dot. Image adapted from [1].

As in the single dot case, the so called charge stability diagram provide a lot of inside into the state of the dots, see Figure 2a for a typical diagram for double dots with no applied applied external bias $V_{\text{SD}}$ [1]. A clear hexagonal pattern is visible compared to the diamonds of the single dot case. The red and blue dots refers to combinations of the gate voltages where the chemical potentials line up, and electrons can flow from source to drain (red), or holes from drain to source (blue) [1].

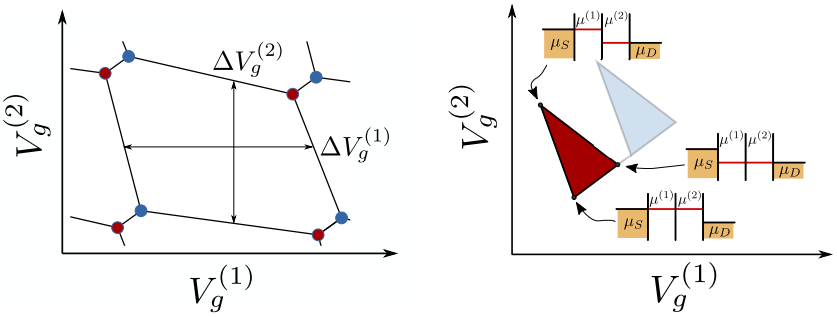


(a) (b)

Figure 2: Charge stability diagram of DQD (a), where red dots represent aligned chemical potentials that allow for electron (red) and hole (blue) transfer. Scaled up view of the dots when a bias $V_{\text{SD}}$ is applied (b), the red and blue (faded) regions correspond to electron and hole transfer.

Furthermore, when an external bias is applied, in this case $V_{\text{SD}} > 0$ the red and blue dots corresponding to a current through the device expand into triangle shaped regions, as seen in Figure 2b [1]. The triangle vertices correspond to a particular potential described by the inset figures [1]. Along the left edge $\Delta\mu^{(1)} = 0$, whilst along the right $\Delta\mu^{(2)} = 0$, and for the base both potentials vary.

## 1.1 Electrostatic Model of DQDs

Weil, et al. provides a classical description of the chemical potential $\mu^{(1)}(N_1, N_2)$, $\mu^{(2)}(N_1, N_2)$ for dot 1 and 2 respectively, where $N_1$,$N_2$ denotes the electron count on each dot [1]

$$\begin{aligned}\mu^{(1)}(N_1, N_2) &= \left(N_1 - \frac{1}{2}\right) E_c^{(1)} + N_2 E_c^{(m)} \\ &\quad - \frac{1}{|e|}\left(C_g^{(1)} V_g^{(1)} E_c^{(1)} + C_g^{(2)} V_g^{(2)} E_c^{(m)}\right), \qquad (1)\\ \mu^{(2)}(N_1, N_2) &= \left(N_2 - \frac{1}{2}\right) E_c^{(2)} + N_1 E_c^{(m)} \\ &\quad - \frac{1}{|e|}\left(C_g^{(1)} V_g^{(1)} E_c^{(m)} + C_g^{(2)} V_g^{(2)} E_c^{(2)}\right). \qquad (2)\end{aligned}$$

Note that the *addition energy*, or the energy to deposit an electron is $\mu^{(1)}(N_1 + 1, N_2) - \mu^{(1)}(N_1, N_2) = E_c^{(1)}$, and vice versa for dot 2. That is, the *addition*

*energy* and the charging energy of each dot are equivalent. This is true only in the classical description and not when quantum effects are considered [1].

Moreover, (1), (2) can be used to estimate the width $\Delta V_g^{(1)}$ and height $\Delta V_g^{(2)}$ of regions in the stability diagram, where for instance $\Delta V_g^{(1)}$ corresponds to the voltage having to be applied to gate (1) such that one more electron can fit on the dot, or

$$\mu^{(1)}(N_1+1, N_2; V_g^{(1)} + \Delta V_g^{(1)}, V_g^{(2)}) = \mu^{(1)}(N_1, N_2; V_g^{(1)}, V_g^{(2)}) \\ \Leftrightarrow \Delta V_g^{(1)} = \frac{|e|}{C_g^{(1)}}, \tag{3}$$

and correspondingly for $\Delta V_g^{(2)}$.

Now, considering the influence of a small change to the voltage of gate $(j)$ on the chemical potential $\mu^{(i)}$ of dot $(i)$, the so called *lever arm*

$$\alpha_{ij} := -\frac{\partial \mu^{(i)}}{\partial V_g^{(j)}}, \tag{4}$$

is obtained, which is a measure of cross-influence between gates and dots [1, 2]. Inserting (1),(2) into (4) yields

$$\alpha_{11} := \frac{1}{|e|} C_g^{(1)} E_c^{(1)}, \tag{5}$$

$$\alpha_{22} := \frac{1}{|e|} C_g^{(2)} E_c^{(2)}, \tag{6}$$

$$\alpha_{12} := \frac{1}{|e|} C_g^{(2)} E_c^{(m)}, \tag{7}$$

$$\alpha_{21} := \frac{1}{|e|} C_g^{(1)} E_c^{(m)}, \tag{8}$$

note the dependence on $E_c^{(m)}$ for cross-terms (7), (8).

Another important note relating to the lever arms $\alpha_{ij}$ is the fact that, as Taubert et al. shows, they have the following relation to the slope of the triangle edges formed when a fixed bias $V_{\mathrm{SD}}$ is applied [2]

$$\alpha_{11} = -s_1 \alpha_{12}, \tag{9}$$

$$\alpha_{22} = \frac{|eV_{\mathrm{SD}}|}{\Delta V_g^{(2)}} \frac{s_1}{s_1 - s_2}, \tag{10}$$

$$\alpha_{12} = \frac{s_{12} - s_2}{s_{12} - s_1} \alpha_{22}, \tag{11}$$

$$\alpha_{21} = -s_2 \alpha_{22}. \tag{12}$$

# 2 Measurements and Procedure

Transport measurements were performed by David Barker [3] on a similar nanowire DQD device to that shown in Figure 3, where (a) shows a schematic representation of the wire whilst (a)-(d) show varying stages of processing. A positive voltage bias of $V_{\mathrm{SD}} = 0.3\,\mathrm{mV}$ was used.

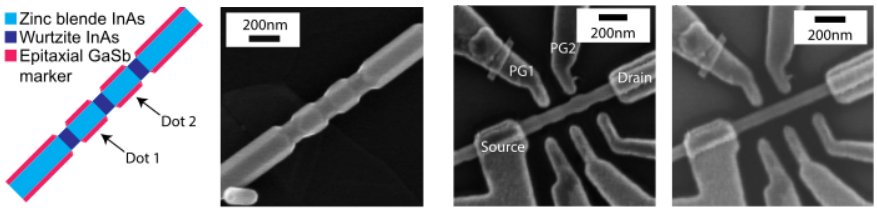


(a) (b)

Figure 3: (a) Schematic of nanowire showing differing materials, and a SEM image of such a nanowire. (b) shows a SEM image of device in (a) before and after Epitaxial GaSb markings had been removed. Image taken from Ref. [3].

From the measurements a stability diagram could be produced and the theory in Sec. 1.1 provided estimates for various charge properties of the DQD.

# 3 Measured Stability Diagrams

Figure 4a presents a large scale view of the measured charge stability diagram for an applied bias of $V_{\mathrm{SD}} = 0.3\,\mathrm{mV}$. In the figure, the width $\Delta V_g^{(1)}$ and height $\Delta V_g^{(2)}$ are indicated. Furthermore, Figure 4b shows a zoomed-in view of a triangle with non-zero current, the slopes of the sides of the triangle along with the total height $\Delta V_{g,small}^{(2)}$ are presented in the figure.

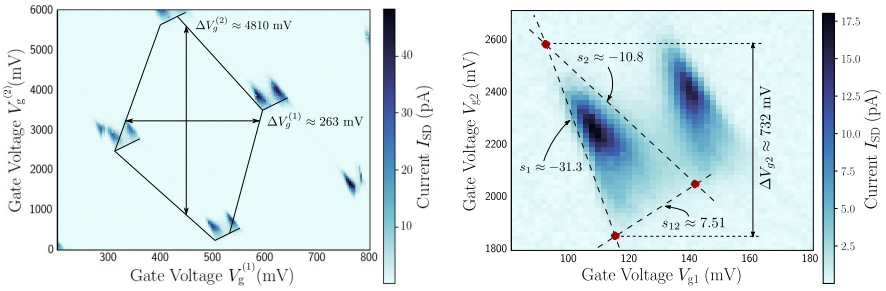


(a) (b)

Figure 4: Large scale charge stability diagram (a) with estimated width $\Delta V_g^{(1)} \approx 263\,\mathrm{mV}$ and height $\Delta V_g^{(2)} \approx 4810\,\mathrm{mV}$ of the stability region; and zoomed in current triangle with calculated slopes $s_1$, $s_2$, and $s_{12}$ along with total triangle height $\Delta V_{g,small}^{(2)} \approx 732\,\mathrm{mV}$.

From Figure 4a and the included width and height of the stability region,

the gate capacitances can be found according to (3)

$$\Delta V_g^{(1)} = \frac{|e|}{C_g^{(1)}} \approx 263\,\text{mV} \Rightarrow C_g^{(1)} \approx 0.609\,\text{aF}, \tag{13}$$

$$\Delta V_g^{(2)} = \frac{|e|}{C_g^{(2)}} \approx 4810\,\text{mV} \Rightarrow C_g^{(2)} \approx 0.0333\,\text{aF}. \tag{14}$$

Next, from Figure 4b and the included slope data, (9)-(12) give the lever arms as

$$\alpha_{11} \approx 9.24\,\text{meV/V} \tag{15}$$

$$\alpha_{22} \approx 0.626\,\text{meV/V} \tag{16}$$

$$\alpha_{12} \approx 0.295\,\text{meV/V} \tag{17}$$

$$\alpha_{21} \approx 6.76\,\text{meV/V} \tag{18}$$

Finally, the above results for the lever arms and gate capacitances in conjunction with (5)-(8) gives the charging energies as

$$E_c^{(1)} \approx 2.43\,\text{meV}, \tag{19}$$

$$E_c^{(2)} \approx 3.01\,\text{meV}, \tag{20}$$

$$E_c^{(m7)} \approx 1.42\,\text{meV}, \tag{21}$$

$$E_c^{(m8)} \approx 1.78\,\text{meV}, \tag{22}$$

where $E_c^{(m7,m8)}$ refers to $E_c^{(m)}$ as calculated from (7) and (8) respectively.

# 4 Feasibility of Results

The fact that $\alpha_{11,21} > \alpha_{22,12}$, that is, gate 1 has a roughly $10\times$ larger impact upon electronic states compared to gate 2, this is also evident in Figure 2a where the voltage scales differ by a factor 10. Moreover, $E_c^{(m)}$ as calculated from (7) and (8) seem in agreement at least in term of scale. The overall magnitude of results are approximately the same when compared to previous results [1, 2, 3].

Sadly, it is hard to draw any significant conclusion from the calculated data two main reasons. Firstly, the slope of the triangle edges were calculated for a single triangle which is not in the hexagon formed in Figure 2a, this is bound to incur inaccuracies, and secondly more measurements on the data could have been done to form more statistically conclusive results, e.g. include more triangles and hexagons.

# References


[1] W.G. van der Wiel, et al. *Electron transport through double quantum dots.* Reviews of Modern Physics, Volume 75, (2003).

[2] D. Taubert, D. Schuh, W. Wegscheider, and S. Ludwig. *Determination of energy scales in few-electron double quantum dots.* Review of Scientific Instruments 82, 123905 (2011); doi: 10.1063/1.3673003.

[3] D. Barker, et al. *Individually addressable double quantum dots formed with nanowire polytypes and identified by epitaxial markers.* Appl. Phys. Lett. 114, 183502 (2019); doi: 10.1063/1.5089275.